Available online at www.sciencedirect.com
ScienceDirect
Catalysis Today 130 (2008) 231–242
CATALYSIS TODAY
www.elsevier.com/locate/cattod

Naphthalene hydrogenation over a NiMo/γ-Al_2O_3 catalyst: Experimental study and kinetic modelling

Carlos M. Cortés Romero [1], Joris W. Thybaut *, Guy B. Marin

Laboratorium voor Petrochemische Techniek, Universiteit Gent, Krijgslaan 281 S5, B-9000 Gent, Belgium

Available online 30 August 2007

Abstract

A kinetic study of the liquid phase naphthalene hydrogenation over a commercial and sulphided NiMo/γ-Al_2O_3 was performed using experimental data obtained in a Robinson–Mahoney reactor at 523–583 K and 2.0–4.0 MPa. The effect of H_2S on the hydrogenation rate was investigated varying its partial pressure from 0.09 to 0.89 MPa. Under these conditions, an exponential decrease in the hydrogenation rate was observed as the H_2S partial pressure increased. The naphthalene conversion ranged from 6 to 89% with tetralin as the main hydrogenation product with selectivities of at least 89%. Reaction networks were formulated based on stepwise hydrogenation mechanisms assuming that both hydrogen and hydrogen sulphide could be dissociated either homolytically or heterolytically on both coordinatively unsaturated metal ion sites (CUS) and sulphur anions (SA) of the sulphided catalyst. Langmuir–Hinshelwood rate equations were derived and discriminated through model regression to experimental data. Two models best describe the experimental data according to a statistical analysis and the physical meaning of the parameter estimates. These models correspond to the third hydrogen addition chemisorbed on CUS and supplied from either homolytic or heterolytic hydrogen dissociation, as rate-determining step. The calculated catalyst surface species concentrations indicate that hydrogen and sulphydril groups are the most abundant species under the investigated operating conditions while the hydrocarbons surface concentration is almost negligible.

Keywords: Hydrogenation; Naphthalene; NiMo; Sulphides; Hydrotreating; Kinetic modelling

1. Introduction

Today's refineries face the challenge of improving fuel quality since current and future environmental regulations prescribe low sulphur, nitrogen and aromatics concentration, particularly in gasoline and diesel. Hydroprocessing technologies offer flexibility to process heavy feedstocks into more valuable products such as transportation fuels [1]. Modifications to these technologies have to be performed to meet the new stringent fuel quality standards with industrial unit reconfiguration and catalyst improvement as the most likely modifications. Both modifications demand a deep knowledge of the chemical phenomena occurring during the catalytic process.

Over the last years, experimental [2–4] and computational investigations [5–8] have provided many insights into the nature of the active phase on hydrotreating catalysts. These catalysts consist of well-dispersed MoS_2 nanocrystallites supported on γ-alumina and promoted by cobalt or nickel atoms. It is generally accepted that the catalytically active sites of sulphided catalysts are located at the edges of the surface. These sites are related to unsaturated metal ions at the Mo-edge, and to the chemisorbed sulphur atoms at the S-edge. It is believed that promoter atoms such as Ni and Co increase the catalytic activity of MoS_2-based catalyst by creating sulphur vacancies with a slightly different electronic structure than those in unpromoted MoS_2 [9–13]. However, even with the recent and better understanding of the sulphided catalysts nature, the exact location of these promoter atoms and their specific role on promotion effect are still under debate since they affect the degree of surface sulphur coverage, which also depends on the operating conditions [9].

Investigations on the hydrogen activation and hydrogen sulphide chemisorption on sulphided catalysts have lead to

* Corresponding author. Fax: +32 9 264 49 99.
E-mail address: Joris.Thybaut@UGent.be (J.W. Thybaut).
[1] Present addres: Mexican Petroleum Institute, Lazaro Cardenas 152, Mexico City 07730, Mexico.

0920-5861/$ – see front matter
doi:10.1016/j.cattod.2007.06.074

Nomenclature

A	pre-exponential factor
A_i	peak surface area of compound i
C_i	concentration of compound i (mol m^{-3} or mol kg_{cat}^{-1})
CUS	coordinatively unsaturated site
E_a	activation energy (kJ mol^{-1})
f_i^L	liquid phase fugacity of component i (bar)
F	experimental molar flow rate (mmol s^{-1})
H°	standard enthalpy (kJ mol^{-1})
k	rate coefficient (mmol s^{-1} bar^{-1})
K	equilibrium coefficient
K	chemisorption equilibrium coefficient (bar^{-1})
nob	number of observations
N	naphthalene
NH_n	partial hydrogenated product, n = 1, 2, 3
p_t	total pressure (bar)
R	reaction rate (mol)
S	selectivity
S°	standard entropy (J mol^{-1} K^{-1})
SSQ	sum of squares
T	tetralin
V_m^L	liquid molar volume (m^3 mol^{-1})
W	catalyst mass (kg)
X	conversion
Y_i	product yield of component i
*	coordinatively unsaturated metal sites (CUS)
$^\bullet$–S^{2-}	sulphur anion sites

Greek symbols

Θ_i	fractional surface coverage of species i
$\gamma_{H2/N}$	molar hydrogen to naphthalene ratio
Δ	difference
δ	sum of surface coverages independent of ratio of free to protonated sulphur anion sites
μ	sum of surface coverages dependent of ratio of free to protonated sulphur anion sites

Superscripts

^	model calculated value
comp	composite
0	inlet value

Subscripts

a	activation
A → B	reaction step from A to B
eq	overall equilibrium
i	species index
j	experimental observation index
k	element in Jacobian matrix
t	total
0	initial concentration

different conclusions regarding the type of dissociation that these molecules undergo on this kind of catalysts, i.e., H_2 and H_2S dissociative chemisorption can be either homolytic or heterolytic. In the first case, bridged S atoms $(S_2)^{2-}$, identified from Raman spectroscopy experiments in Mo–S–S–Mo structures, were suggested as probable sites for homolytic H_2 dissociation [14]. Also, theoretical investigations indicated that these bridged S atoms facilitate the homolytic dissociation due to an electronic charge transfer between the sulphur atom and the hydrogen antibonding σ* orbital leading to two practically equivalent S–H species [15]. The heterolytic dissociation of hydrogen is supported by deuterium tracer experiments on sulphided catalysts [4,16] and theoretical calculations on promoted and unpromoted MoS_2 [7,17]. In summary, these studies established the formation of $(metal–H)^-$ and $(S^{2-}–H^+)$ species as the most stable on a catalyst surface where the sulphur coverage is lower or equal to 50%, depending on the operating conditions and the promoter content of the catalyst. The homolytic dissociation of hydrogen to two S–H groups is preferred on a fully sulphided S-edge as well as on a fully sulphided Mo-edge, whereas the heterolytic dissociation that yields Mo–H and S–H is more likely to occur on a partially sulphided edge [9].

The chemical phenomena in hydrotreating of complex feedstocks at industrial operating conditions are complex. Hence, HDS, HDN and HYD are being investigated using model components at operating conditions where intrinsic kinetics can be measured. For instance, kinetic studies of toluene hydrogenation [18,19] and dibenzothiophene desulphurization [20] over sulphided $NiMo/Al_2O_3$ at wide operating conditions in the presence of H_2S and/or NH_3 have led to the postulation of reaction mechanisms involving the sequential addition of chemisorbed hydrogen dissociated either homolytically or heterolytically. For the toluene case, the model discrimination was performed by the qualitative observed trends assuming different partial reaction orders for the reactants and especially for H_2S. In general, the kinetic models developed are used in the simulation of an industrial hydrotreating reactor, to evaluate the process performance as a function of the operating conditions or as a function of the feed composition [21–23].

Studies indicate that the extent of particles emissions in diesel exhaust can be reduced by (i) decreasing the sulphur content; (ii) increasing the cetane-number; and (iii) decreasing the aromatic content [24,25]. In this work hydrogenation is focused on as an important reaction in the efficient production of environmental friendly fuels. Hydrogenation is of increasing interest for petroleum refiners to comply with future environmental policies. Mechanistic considerations occurring during the liquid phase aromatics hydrogenation are investigated using naphthalene as model molecule over a sulphided NiMo catalyst at conditions where intrinsic kinetics can be measured. The rate equations are derived assuming each atomic or ionic hydrogen addition as possible rate-determining step based on the Langmuir–Hinshelwood formalism. The model selection is performed by the analysis of the statistical results of the model regression and on the basis of the physical meaningfulness of the parameter estimates.

2. Procedures

2.1. Catalyst and materials

A commercial NiMo/γAl_2O_3 catalyst, PROCATALYSE EC220/99/23, was used for the experimental naphthalene hydrogenation. This catalyst contains 9.3 wt.% Mo and 2.5 wt.% Ni. The specific volume amounts to 4.94×10^{-4} m^3 kg^{-1}, its specific surface area is 1.90×10^5 m^2 kg^{-1} and its mesoporous volume 7.70×10^{-4} m^3 kg^{-1}. Typically, 2.0×10^{-3} kg of catalyst was used with a diameter between 5.6 and 6.0×10^{-3} m, dried at 393 K during 14.4 ks and sulphided in situ at 653 K, 0.1 MPa and 27.2 mol s^{-1} of H_2S/H_2 commercial mixture (Air Liquide-Alpha Gaz, 10 mol% H_2S) during 28.8 ks.

The liquid chemicals, i.e., naphthalene (Acros Org anics, 202049-5, 99%), and dimethyldisulphide (Aldrich 32041-2, 99%) and the gases, i.e., H_2 and CH_4 (Air Liquide, 99.9%) and the H_2S/H_2 mixture (Air Liquide-Alpha Gaz) were used without further purification. A commercial mixture of *n*-paraffins denoted as Halpasol 190/240 (Haltermann Products) was used as solvent. The GC/FID analysis of this solvent indicated a distribution of paraffins as follows (wt.%): 0.14 *n*-nonane, 9.31 *n*-decane, 35.0 *n*-undecane, 30.8 *n*-dodecane, 23.4 *n*-tridecane, 1.17 *n*-tetradecane, 0.10 *n*-pentadecane and 0.08 *n*-hexadecane.

2.2. Set-up and operating conditions

Naphthalene was hydrogenated in a three-phase Robinson–Mahoney reactor which is of the CSTR type. The schematic representation of the set-up currently used and the operating procedure of the Robinson–Mahoney reactor have been reported in previous works from our group [21,26]. The investigated range of temperatures was 523–583 K, of total pressures 2.0–4.0 MPa, of space times 0.88–3.53 kg s mmol^{-1}, of inlet naphthalene concentrations 2.6–5.6 mol%, of inlet molar hydrogen to naphthalene ratios ($\gamma_{H_2/N}$) 9–29 and of inlet molar H_2/H_2S ratios 5–40. These operating conditions lead to a H_2S partial pressure range from 0.08 to 0.90 MPa. The H_2S partial pressure was controlled by addition of dimethyldisulphide (DMDS) to the liquid feed. DMDS was assumed to decompose instantaneously upon contacting the catalyst.

The operating conditions, together with the reactant and reactor type have been selected to measure *intrinsic* kinetics, i.e., free from any transport limitations and flow non-idealities.

2.3. Analytical section, data treatment and reproducibility

Both gas and liquid phases were analysed using a Gas-Chromatograph CHROMPACK CP-9001. The liquid feedstock and product were analysed using a flame ionization detector (FID) with a 50 m WCOT fused silica capillary column using helium as carrier gas. The analysis program started at 393 K for 7 min followed by a ramp of 4 °C min^{-1} till 463 K. Gas feedstock and product were analysed using a 1 m HAYSEP N packed column at 393 K with a thermal conductivity detector (TCD) using N_2 as carrier and reference gas. An FID analysis of the gas product was not required since it only contains H_2, H_2S and CH_4 and no heavier hydrocarbons. Methane was used as internal standard to accurately determine the individual component flow rates in the gas feed and gas reactor effluent. A constant inlet molar hydrogen to methane ratio of 6.5 was maintained for the entire set of experiments. The composition of the liquid feed and product was obtained using calibration factors determined by a method described by Dierickx et al. [27]. The molar flow rate of each component of the flashed gas and liquid reactor effluents was calculated using the normalized composition obtained from GC analysis (mol m^{-3}) and the volumetric hourly liquid and gas flow rates measured at steady-state conditions (m^3 s^{-1}). Only those experimental data were retained in which the total mass, carbon, hydrogen and sulphur balance ranged from 95 to 105%.

The fractional naphthalene conversion was calculated by:

$$X_N = \frac{F_N^0 - F_N}{F_N^0} \quad (1)$$

where F_N^0 and F_N represent the naphthalene inlet and outlet molar flow rates in the liquid phase.

Selectivities to products such as tetralin and decalins were calculated by:

$$S_i = \frac{F_i}{F_N^0 - F_N} \quad (2)$$

where F_i is the outlet molar flow rate of hydrogenation product.

The yield of products were calculated as

$$Y_i = \frac{F_i}{F_N^0} = S_i X_N \quad (3)$$

Catalyst performance reproducibility was verified by monitoring reference experiments on two different catalyst batches immediately after presulphiding and on the same catalyst batch after performing a set of experiments and intermittent shut-down of the set-up, vide Fig. 1. Whenever the

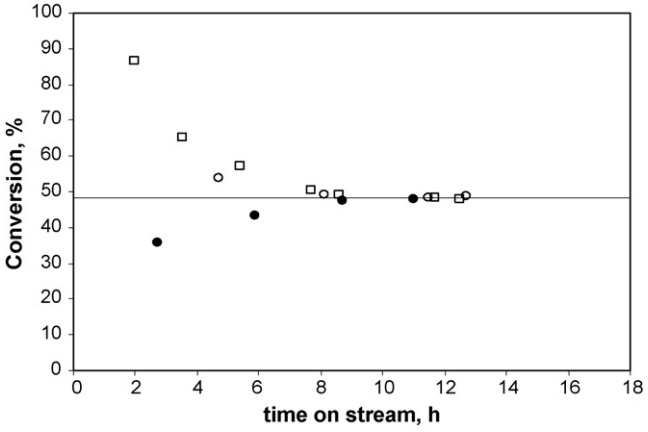

Fig. 1. Reproducibility and stabilization time in naphthalene hydrogenation using two different catalyst batches (□ and ○) immediately after presulphiding and after having performed a set of experiments and intermittent set-up shut-down (●) at reference conditions, i.e., 553 K, 4.0 MPa, C_N^0 2.6 mol%, W/F_N^0 1.76 kg s mmol^{-1}, inlet H_2/H_2S molar ratio 40 and inlet H_2/naphthalene molar ratio 15.5.

catalyst was freshly activated, the initial hydrogenation conversion was high and then dropped to the steady-state regime values. In general, the time for reactor and reaction stabilization depended on the volumetric liquid flow rate. At the reference conditions, the steady-state regime was reached after 8 h on stream. It is worthwhile to mention that slight catalyst deactivation was observed after about 190 h during continuous reactor operation. However, the original activity could be restored by exposing the catalyst to the initial sulphiding procedure [28]. Cracking of the solvent paraffins was not observed within the operating conditions applied. The entire set of experimental data amounted to 121.

2.4. Equilibrium calculations and kinetic regime verification

In order to verify that the experimental data were not limited by thermodynamics within the investigated temperature range, a simultaneous chemical and phase equilibrium simulation was performed using literature reported thermodynamic data and the Peng–Robinson equation of state [29]. Full hydrogenation of naphthalene is expected at the current conditions according to the calculated product distribution depicted in Fig. 2. The highest experimentally observed naphthalene conversion amounted to 89% which is lower than that predicted by equilibrium and, hence, no limitation from thermodynamics can be inferred. With respect to the phase equilibrium, the calculations predict an average liquid evaporation of 13% by increasing the temperature by 30 °C from 553 to 583 K at a total pressure of 2.0 MPa. This liquid evaporation drops to 2.5% when a total pressure of 4.0 MPa is used. Based on these results, experiments were planned at sufficiently low temperatures and high pressures.

Mass and heat transfer gradients were evaluated with special care for the experiments where the observed rate was high. Several criteria were used for the assessment of transport limitations [30–34]. Mass transfer limitations at the gas phase side could be considered negligible [30]. Mass transport of hydrogen at the gas–liquid interphase and of both hydrogen and naphthalene at the liquid–solid interphase were assessed by calculating dimensionless Carberry's numbers [30,31]. The most critical value of the Carberry's number corresponded to H_2 mass transfer from gas to liquid and reached 0.03 assuming a partial first reaction order with respect to this reactant. This value is lower than that assumed as the limit (0.05) for first-order kinetics.

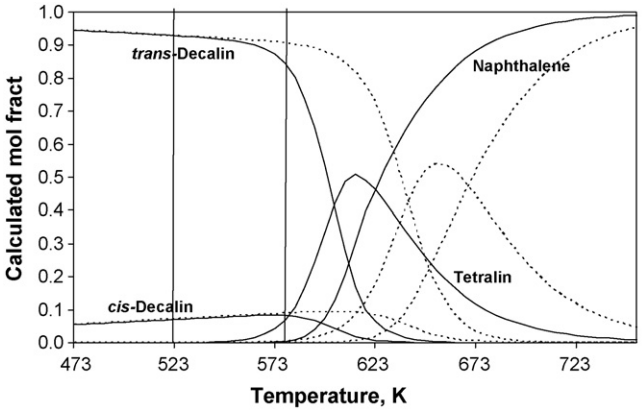

Fig. 2. Thermodynamic equilibrium distribution as a function of temperature at C_N^0 2.56 mol% in Halpasol, inlet H_2/H_2S molar ratio 40, inlet $\gamma_{H_2/N}$ ratio 15.5, total pressure 2 MPa (solid lines) and 4 MPa (dotted lines). Vertical lines: investigated temperature range.

The importance of intraparticle diffusion limitations was assessed with the Weisz–Prater criterion [33]. The effectiveness factor of both hydrogen and naphthalene were close to the unity (0.97) with the most critical Weisz modulus (Φ) value of 0.052 for naphthalene which still was lower than that established as limit (0.08) assuming first-order kinetics.

The absence of heat transfer limitations was verified by using diagnostic criteria reported by Mears [32]. Both external and internal temperature gradients were found to be lower than the corresponding established limits, e.g. at the liquid–solid interphase the ΔT_{LS} was 0.14 K while the limit is 0.63 K. Isothermicity into the particle was also observed since the calculated ΔT_{int} was at least one order of magnitude lower than the limit, i.e., 0.05 K compared to 0.63 K.

2.5. Parameter estimation procedure

Parameter estimation was performed by minimization of the sum of squares of the residuals between the experimental and calculated molar outlet molar flow rate of tetralin using a combination of a Rosenbrock and a Marquardt algorithm [35,36].

$$\mathrm{SSQ} = \sum_{j=1}^{\mathrm{nob}} (F_{\mathrm{T},j} - \hat{F}_{\mathrm{T},j})^2 \rightarrow \min \tag{4}$$

An in-house code was used for the Rosenbrock method, while for the Marquardt algorithm the ordinary least square (OLS) option of the ODRPACK-package version 2.01 was used [37]. For a given net rate of production $\hat{R}_T$, the tetralin outlet flow rate $\hat{F}_{T,j}$ is calculated by solving the following algebraic equation:

$$\hat{F}_{\mathrm{T},j} - \hat{R}_{\mathrm{T}}(T, p, \hat{F}_{\mathrm{T},j}, F_{\mathrm{N}}^0) W_j = 0 \tag{5}$$

i.e., via the mass balance for tetralin over the reactor.

The iterative procedure for parameter estimation began by performing simulations to obtain good initial guesses of the parameters. Once simulations results were within one order of magnitude of the experimental ones, an optimization procedure was established in which successive iterations first with the Rosenbrock algorithm for a rough estimation and afterwards with the Marquardt one for a more refined estimation was the modus operandi. The model discrimination was based on the physical meaning of the parameters and by comparison of the global regression results through the obtained F-value. First, isothermal model regression was performed using the experimental data set obtained at 553 K, the reference temperature. The remaining models were then tested for the entire set of experimental data at different temperatures by expressing the temperature dependency of the model para-

meters applying the Arrhenius and Van't Hoff equations for the rate and chemisorption coefficients, respectively [38].

The statistical significance of the global regression is expressed by means of the so-called F-test, which is based on the comparison of the calculated sum of squares of the calculated response value and the residual sum of squares. A high F-value corresponds to a high significance of the global regression. The parameter estimates were tested for statistical significance on the basis of their individual t-values and 95% confidence intervals [39].

2.6. Vapour–liquid equilibrium calculations

The liquid phase kinetics are expressed in terms of fugacities, i.e., the ideal gas state is used as reference state [40]. The fractional surface coverages of reactant species are obtained from the liquid phase fugacities through a Langmuir isotherm:

$$\Theta_i = \frac{K_i f_i^{\mathrm{L}}}{1 + K_i f_i^{\mathrm{L}}} \tag{6}$$

where f_i^{L} stands for liquid phase fugacity of chemisorbing species i. The relationship between fugacities and liquid phase concentrations is given by the following equation:

$$f_i^{\mathrm{L}} = \Phi_i^{\mathrm{L}} p_{\mathrm{t}} V_{\mathrm{m}}^{\mathrm{L}} C_i^{\mathrm{L}} \tag{7}$$

where p_{t} is the total pressure, $V_{\mathrm{m}}^{\mathrm{L}}$ the liquid molar volume, C_i^{L} the molar concentration of A in liquid phase and Φ_i^{L} is the fugacity coefficient of species i in liquid phase calculated as described elsewhere [29].

3. Experimental results

Within the investigated range of reaction conditions, tetralin was the main product of naphthalene hydrogenation with selectivities above 89% as it is depicted in Fig. 3. In most of the experimental data the selectivity to tetralin even exceeded 95%. The other hydrogenation products were decalins with a *trans* to *cis* ratio of about 3. Neither partially hydrogenated products such as hexahydro- and octahydro-naphthalene nor isomerization nor ring opening products were detected during the experimentation. Therefore, for all practical purposes, the present study can be limited to the selective hydrogenation from naphthalene to tetralin.

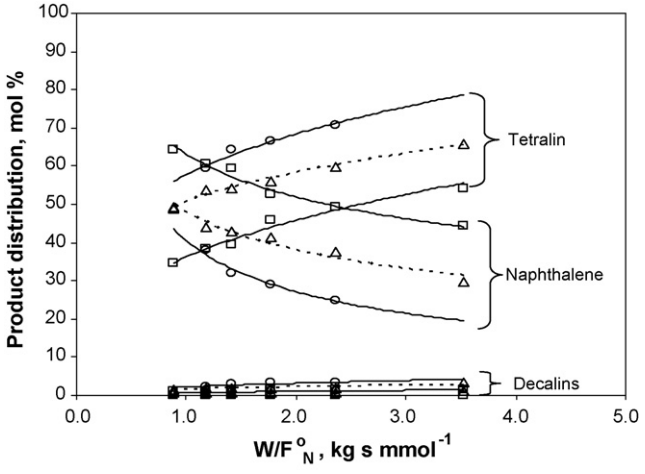

Fig. 3. Product distribution as function of space time for 2.6 mol% (□), 4.5 mol% (△) and 5.7 mol% (○) of inlet naphthalene concentrations. Lines: observed trend. Conditions: 553 K, 4.0 MPa, inlet H_2/H_2S molar ratio 40 and inlet $\gamma_{H_2/N}$ ratio 15.5.

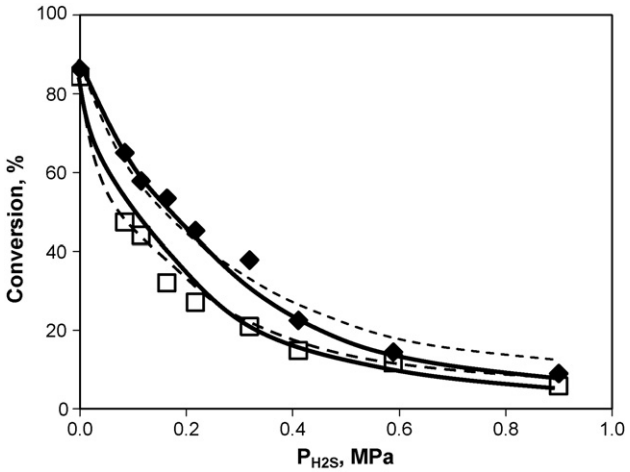

Fig. 4. Naphthalene conversion vs. P_{H_2S} for 2.6 mol% (□) and 4.5 mol% (◆) of inlet naphthalene concentration at 553 K, 4.0 MPa, inlet H_2/H_2S molar ratio 40 and inlet $\gamma_{H_2/N}$ ratio 15.5. Symbols: experimentally observed values; lines: model calculated values using model 3-H-CUS (solid lines) and 3-Hydride (dotted lines) in Table 4 with the set of parameter estimates given in Tables 7 and 8.

A negative effect of H_2S on the hydrogenation conversion is observed as its inlet concentration increases, vide Fig. 4. The investigated range of inlet molar H_2/H_2S ratios varied from 5 to 40, which encompasses the range industrially applied in hydrotreating units, i.e., from 30 to 40 [41]. The naphthalene conversion drops sharply as the H_2S partial pressures increases from 0 to approximately 0.18 MPa. The negative effect is more moderate as the H_2S partial pressure further increases until a value of 0.40 MPa. From this value on, almost no effect was observed on the hydrogenation conversion regardless the initial naphthalene concentration. This is an indication that the H_2S chemisorption on the catalyst surface ranges from the Henry's regime, i.e., from low surface concentration, to the saturation regime. These results are in agreement with those reported for toluene hydrogenation over MoS_2/Al_2O_3, in which the change in slope of the curve was interpreted in terms of different partial reaction orders with respect to H_2S depending on its concentration during the reaction [18].

The inlet molar hydrogen to naphthalene ratio, $\gamma_{H_2/N}$, has a positive effect on the hydrogenation conversion for the two different inlet naphthalene concentrations considered, vide Fig. 5. This effect is slightly more pronounced at the highest inlet naphthalene concentration. $\gamma_{H_2/N}$ was varied by changing the inlet molar hydrogen flow rate, keeping that of naphthalene, and consequently that of DMDS, fixed. As a result, in the range of $\gamma_{H_2/N}$ investigated, the H_2 partial pressure increased from 3.23 to 3.39 MPa while that of H_2S decreased from 0.16 to

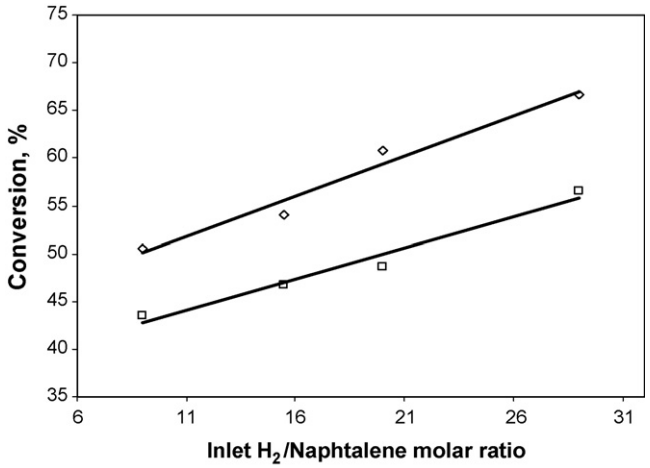

Fig. 5. Naphthalene conversion vs. inlet $\gamma_{H_2/N}$ ratio for 2.6 mol% (□) and 4.5 mol% (◇) of inlet naphthalene concentrations, 553 K, 4.0 MPa, 1.76 kg s mmol^{-1}. Lines: observed trend.

0.04 MPa. The increase in the H_2 partial pressure implies an increase in the hydrogen concentration in the liquid phase. However, it can be inferred from the discussion above that the decrease in H_2S partial pressure also significantly contributes to the enhanced hydrogenation rates through a reduction of the H_2S inhibition effect. At higher naphthalene concentrations, the effect of the inlet molar hydrogen to naphthalene ratio $\gamma_{H_2/N}$ on the naphthalene conversion is somewhat more pronounced because of the positive partial reaction order for naphthalene.

4. Kinetic analysis

4.1. Model assumptions

The modelling of the naphthalene hydrogenation was based on the following assumptions in which both the experimental results discussed in the previous section and the insight on the nature of the sulphided catalyst reported in literature were accounted for:

(i) only the first hydrogenation stage, i.e., from naphthalene to tetralin, is considered;
(ii) two reaction mechanisms are proposed according to the mode of the dissociative chemisorption that H_2 and H_2S undergo on the active sites of the sulphided catalyst: homolytic or heterolytic;
(iii) the stepwise hydrogenation mechanism proceeds via successive hydrogen additions either from coordinatively unsaturated sites (CUS) or from sulphur anions (SA), i.e., [*] or [$^{\bullet}$–S^{2-}]. This results in the following atomic hydrogen species, i.e., *–H or $^{\bullet}$–S^{2-}H, or ionic hydrogen species, i.e., *–H^- or $^{\bullet}$–$S^{2-}H^+$, available for addition to the aromatic ring;
(iv) the chemisorption of hydrocarbon species, e.g. naphthalene and tetralin, can only occur on CUS. This assumption is supported by the electronic nature of this interaction;
(v) dissociative chemisorption of H_2S involves both types of active sites: CUS binds the sulphydril group, i.e., *–SH or *–SH^-, and SA are the host for the hydrogen or proton, viz $^{\bullet}$–S^{2-}H or $^{\bullet}$–$S^{2-}H^+$, depending on the type of dissociation.
(vi) no interconversion of active sites is considered because the sulphydril on a CUS is electronically different from a hydrogen atom or proton chemisorbed on a SA [8–11]:

$$*-\mathrm{SH} \neq {}^{\bullet}-\mathrm{S^{2-}H} \text{ and } *-\mathrm{SH^-} \neq {}^{\bullet}-\mathrm{S^{2-}H^+} \quad (8)$$

4.2. Rate equation derivation

The current notation for the active CUS and sulphur anions, i.e., * and $^{\bullet}$–S^{2-}, is equivalent to the previously used notation, i.e., τ and σ [21–23], however, the currently used one is considered to be more instructive. The set of elementary reactions for naphthalene hydrogenation is presented in Table 1 for the homolytic mechanism and in Table 2 for the heterolytic one.

Applying the Langmuir–Hinshelwood–Hougen–Watson (LHHW) formalism and considering each reversible hydrogenation step as possibly rate determining leads to 16 rate equations. The methodology for deriving a rate equation is based on that reported by Kasztelan et al. [18]. In what follows, as an example, the key points are described in the derivation of an equation corresponding to a heterolytic reaction network in which a hydride species addition occurs first.

The site balances for both types of active sites are:

$$C_{t,*} = C_* + C_{*-\mathrm{H^-}} + C_{*-\mathrm{SH^-}} + C_{*-\mathrm{N}} + C_{*-\mathrm{NH^-}} + C_{*-\mathrm{NH_2}} + C_{*-\mathrm{NH_3^-}} + C_{*-\mathrm{T}} \quad (9)$$

$$C_{t,{}^{\bullet}-\mathrm{S^{2-}}} = C_{{}^{\bullet}-\mathrm{S^{2-}}} + C_{{}^{\bullet}-\mathrm{S^{2-}H^+}} \quad (10)$$

A third balance expresses the conservation of electrical charge:

$$C_{t,(-)} = 2C_{{}^{\bullet}-\mathrm{S^{2-}}} + C_{{}^{\bullet}-\mathrm{S^{2-}H^+}} + C_{*-\mathrm{H^-}} + C_{*-\mathrm{SH^-}} \quad (11)$$

Table 1
Elementary steps in the naphthalene hydrogenation mechanism on a sulphided NiMo catalyst considering homolytic dissociation of hydrogen and hydrogen sulphide

	Coefficient[a]
Chemisorption/desorption equilibria	
$N + * \rightleftarrows * - N$	K_N
$H_2 + 2* \rightleftarrows 2* - H$	$K_{H_2,*}$
$H_2 + 2{}^{\bullet}-S^{2-} \rightleftarrows 2{}^{\bullet}-S^{2-}H$	$K_{H_2,{}^{\bullet}-S^{2-}}$
$H_2S + * + {}^{\bullet}-S^{2-} \rightleftarrows * - SH + {}^{\bullet}-S^{2-}H$	K_{H_2S}
$T + * \rightleftarrows * - T$	K_T
Hydrogenation network via *–H addition only	
$*-N + *-H \rightleftarrows * - NH_2 + *$	$K_{N\rightarrow NH,*}$
$*-NH + *-H \rightleftarrows * - NH_2 + *$	$K_{NH\rightarrow NH_2,*}$
$*-NH_2 + *-H \rightleftarrows * - NH_3 + *$	$K_{NH_2\rightarrow NH_3,*}$
$*-NH_3 + *-H \rightleftarrows * - T + *$	$K_{NH_3\rightarrow T,*}$
Hydrogenation network via $^{\bullet}$–S^{2-}H addition only	
$*-N + {}^{\bullet}-S^{2-}H \rightleftarrows * - NH + {}^{\bullet}S^{2-}$	$K_{N\rightarrow NH,{}^{\bullet}-S^{2-}}$
$*-NH + {}^{\bullet}-S^{2}H \rightleftarrows * - NH_2 + {}^{\bullet}-S^{2-}$	$K_{NH\rightarrow NH_2,{}^{\bullet}-S^{2-}}$
$*-NH_2 + {}^{\bullet}-S^{2}H \rightleftarrows * - NH_3 + {}^{\bullet}-S^{2-}$	$K_{NH_2\rightarrow NH_3,{}^{\bullet}-S^{2-}}$
$*-NH_3 + {}^{\bullet}-S^{2-}H \rightleftarrows * - T + {}^{\bullet}-S^{2-}$	$K_{NH_3\rightarrow T,{}^{\bullet}-S^{2-}}$

[a] N: naphthalene ($C_{10}H_8$), NH_n: further hydrogenated products until T: tetralin ($C_{10}H_{12}$).

Table 2
Elementary steps in the naphthalene hydrogenation mechanism on a sulphided NiMo catalyst considering heterolytic dissociation of hydrogen and hydrogen sulphide

	Coefficient[a]
Chemisorption/desorption equilibria	
$N + * \rightleftarrows * - N$	K_N
$H_2 + * + {}^{\bullet}\!-S^{2-} \rightleftarrows * - H + {}^{\bullet}\!-S^{2-}H^+$	K_{H_2}
$H_2S + * + {}^{\bullet}\!-S^{2-} \rightleftarrows * - SH + {}^{\bullet}\!-S^{2-}H^+$	K_{H_2S}
$T + * \rightleftarrows * - T$	K_T
Hydrogenation network assuming a hydride addition first ($*\!-\!H^-$)	
$* - N + * - H \rightleftarrows * - NH^- + *$	$K_{N \to NH^-}$
$* - NH^- + {}^{\bullet}\!-S^{2-}H^+ \rightleftarrows * - NH_2 + {}^{\bullet}\!-S^{2-}$	$K_{NH^- \to NH_2}$
$* - NH_2 + * - H \rightleftarrows * - NH_3^- + *$	$K_{NH_2 \to NH_3^-}$
$* - NH_3^- + {}^{\bullet}\!-S^{2-}H^+ \rightleftarrows * - T + {}^{\bullet}\!-S^{2-}$	$K_{NH_3^- \to T}$
Hydrogenation network assuming a proton addition first (${}^{\bullet}\!-S^{2-}H^+$)	
$* - N + {}^{\bullet}\!-S^{2-}H \rightleftarrows * - NH + {}^{\bullet}\!-S^{2-}$	$K_{N \to NH^+}$
$* - NH + * - H^- \rightleftarrows * - NH_2 + *$	$K_{NH^+ \to NH_2}$
$* - NH_2 + {}^{\bullet}\!-S^{2-}H \rightleftarrows * - NH_3^+ + {}^{\bullet}\!-S^{2-}$	$K_{NH_2 \to NH_3^+}$
$* - NH_3^+ + * - H^- \rightleftarrows * - T + *$	$K_{NH_3^+ \to T}$

[a] N: naphthalene ($C_{10}H_8$), NH_n: further hydrogenated products until T: tetralin ($C_{10}H_{12}$).

Eq. (9) can be written as a function of liquid phase concentrations using Eqs. (6) and (7), cf. Section 2.6, and the equilibria presented in Table 2.

$$C_{t,*} = C_* \left(1 + K_{H_2} f_{H_2} \frac{C_{\bullet-S^{2-}}}{C_{\bullet-S^{2-}H^+}} + K_{H_2S} f_{H_2S} \frac{C_{\bullet-S^{2-}}}{C_{\bullet-S^{2-}H^+}} + K_N f_N + K_{N \to NH^-} K_N K_{H_2} f_N f_{H_2} \frac{C_{\bullet-S^{2-}}}{C_{\bullet-S^{2-}H^+}} + K_{N \to NH_2} K_N K_{H_2} f_N f_{H_2} + \frac{K_T f_T}{K_{NH_3^- \to T}} \frac{C_{\bullet-S^{2-}}}{C_{\bullet-S^{2-}H^+}} + K_T f_T \right) \quad (12)$$

The most favourable interaction with the catalyst surface is assumed to occur for the reactant and product hydrocarbons. As a result the hydrocarbon intermediates surface concentrations can be neglected and, hence, the corresponding chemisorption terms in Eq. (12) can be discarded:

$$C_{t,*} = C_* \left(1 + K_{H_2} f_{H_2} \frac{C_{\bullet-S^{2-}}}{C_{\bullet-S^{2-}H^+}} + K_{H_2S} f_{H_2S} \frac{C_{\bullet-S^{2-}}}{C_{\bullet-S^{2-}H^+}} + K_N f_N + K_T f_T \right) \quad (13)$$

The summation in Eq. (13) can be grouped in terms with a $C_{\bullet-S^{2-}}/C_{\bullet-S^{2-}H^+}$ dependence and those independent of this ratio. This leads to the following definitions:

$$\delta = 1 + K_N f_N + K_T f_T \quad (14)$$

$$\mu = K_{H_2} f_{H_2} + K_{H_2S} f_{H_2S} \quad (15)$$

which, incorporated in Eq. (13), lead to:

$$C_{t,*} = C_* \left(\delta + \mu \frac{C_{\bullet-S^{2-}}}{C_{\bullet-S^{2-}H^+}} \right) \quad (16)$$

In order to write the ratio $C_{\bullet-S^{2-}}/C_{\bullet-S^{2-}H^+}$ in terms of known concentrations, an approximation related to the concentration of the active sites is needed:

$$C_{t,\bullet-S^{2-}} = C_{t,*} \quad (17)$$

An identical concentration of sulphur anions and coordinatively unsaturated sites is proposed because saturation of one of the two types of sites would suppress H_2 and H_2S dissociation [18].

According to the H_2S chemisorption stoichiometry the following relationship can be obtained:

$$C_{\bullet-S^{2-}H^+} = C_{*-H^-} + C_{*-SH^-} \quad (18)$$

using expressions for the chemisorption equilibria for H_2 and H_2S, Eq. (18) can be written as:

$$C_{\bullet-S^{2-}H^+} = \sqrt{\mu C_{\bullet-S^{2-}} C_*} \quad (19)$$

The assumption on the equality of the total number of the two types of active sites, Eq. (17), allows to set Eqs. (9) and (10) equal to each other. Accounting for the chemisorption stoichiometry, Eq. (18), and for the low concentration of hydrocarbon intermediates, the following relationship is obtained:

$$C_{\bullet-S^{2-}} = C_* + C_{*-N} + C_{*-T} \quad (20)$$

Using the definition of δ, Eq. (14), this equation can be rewritten as:

$$C_{\bullet-S^{2-}} = \delta C_* \quad (21)$$

and, hence, after substitution in Eq. (19), the following expression is obtained for the ratio of the concentrations of free and protonated sulphur anions:

$$\frac{C_{\bullet-S^{2-}}}{C_{\bullet-S^{2-}H^+}} = \sqrt{\frac{\delta}{\mu}} \quad (22)$$

So far, the site balance for CUS has been further developed without deriving a rate equation. As a result, the expressions derived so far are independent of the step that will be assumed to be rate determining.

As an example the rate equation corresponding to the third hydride addition as rate-determining step will be derived, vide Table 2:

$$*\text{-}NH_2 + *\text{-}H \rightleftarrows *\text{-}NH_3^- + * \qquad R_{NH_3^-,*-H^-} = k_3 \left(C_{*-NH_2} C_{*-H^-} - \frac{C_{*-NH_3^-} C_*}{K_3} \right) \quad (23)$$

Table 3
Rate equations derived from homolytic mechanism assuming each hydrogen addition as possible rate-determining step

Hydrogenation network via *–H addition only		
$*\text{-}N + * \text{-} H \rightleftharpoons * \text{-}NH + *$	$R_{\mathrm{NH},*-\mathrm{H}} = k_1 K_{\mathrm{N}} f_{\mathrm{N}} \sqrt{K_{\mathrm{H}_2,*} f_{\mathrm{H}_2}} \left(1 - \frac{f_{\mathrm{T}}}{K_{\mathrm{eq}} f_{\mathrm{N}} f_{\mathrm{H}_2}^2}\right) C_*^2$	1-H-CUS
$* \text{-} NH + * \text{-} H \rightleftharpoons * \text{-} NH_2 + *$	$R_{\mathrm{NH}_2,*-\mathrm{H}} = k_2 K_{\mathrm{N}\rightarrow\mathrm{NH},*} K_{\mathrm{N}} f_{\mathrm{N}} K_{\mathrm{H}_2,*} f_{\mathrm{H}_2} \left(1 - \frac{f_{\mathrm{T}}}{K_{\mathrm{eq}} f_{\mathrm{N}} f_{\mathrm{H}_2}^2}\right) C_*^2$	2-H-CUS
$* \text{-} NH_2 + * \text{-} H \rightleftharpoons * \text{-} NH_3 + *$	$R_{\mathrm{NH}_3,*-\mathrm{H}} = k_3 K_{\mathrm{N}\rightarrow\mathrm{NH}_2,*} K_{\mathrm{N}} f_{\mathrm{N}} (K_{\mathrm{H}_2,*} f_{\mathrm{H}_2})^{3/2} \left(1 - \frac{f_{\mathrm{T}}}{K_{\mathrm{eq}} f_{\mathrm{N}} f_{\mathrm{H}_2}^2}\right) C_*^2$	3-H-CUS
$* \text{-} NH_3 + * \text{-} H \rightleftharpoons * \text{-} T + *$	$R_{\mathrm{T},*-\mathrm{H}} = k_4 K_{\mathrm{N}\rightarrow\mathrm{NH}_3,*} K_{\mathrm{N}} f_{\mathrm{N}} (K_{\mathrm{H}_2,*} f_{\mathrm{H}_2})^2 \left(1 - \frac{f_{\mathrm{T}}}{K_{\mathrm{eq}} f_{\mathrm{N}} f_{\mathrm{H}_2}^2}\right) C_*^2$	4-H-CUS
Hydrogenation network via $^{\bullet}$–S^{2-}H addition only		
$* \text{-} N + \bullet\text{-} S^{2-} H \rightleftharpoons * \text{-} NH + \bullet\text{-} S^{2-}$	$R_{\mathrm{NH},\bullet-\mathrm{S}^{2-}\mathrm{H}} = k_1 K_{\mathrm{N}} f_{\mathrm{N}} \sqrt{K_{\mathrm{H}_2,\bullet-\mathrm{S}^{2-}} f_{\mathrm{H}_2}} \left(1 - \frac{f_{\mathrm{T}}}{K_{\mathrm{eq}} f_{\mathrm{N}} f_{\mathrm{H}_2}^2}\right) C_* C_{\bullet-\mathrm{S}^{2-}}$	1-H-SA
$* \text{-} NH + \bullet\text{-} S^{2-} H \rightleftharpoons * \text{-} NH_2 + \bullet\text{-} S^{2-}$	$R_{\mathrm{NH}_2,\bullet-\mathrm{S}^{2-}\mathrm{H}} = k_2 K_{\mathrm{N}\rightarrow\mathrm{NH},\bullet-\mathrm{S}^{2-}} K_{\mathrm{N}} f_{\mathrm{N}} K_{\mathrm{H}_2,\bullet-\mathrm{S}^{2-}} f_{\mathrm{H}_2} \left(1 - \frac{f_{\mathrm{T}}}{K_{\mathrm{eq}} f_{\mathrm{N}} f_{\mathrm{H}_2}^2}\right) C_* C_{\bullet-\mathrm{S}^{2-}}$	2-H-SA
$* \text{-} NH_2 + \bullet\text{-} S^{2-} H \rightleftharpoons * \text{-} NH_3 + \bullet\text{-} S^{2-}$	$R_{\mathrm{NH}_3,\bullet-\mathrm{S}^{2-}\mathrm{H}} = k_3 K_{\mathrm{N}\rightarrow\mathrm{NH}_2,\bullet-\mathrm{S}^{2-}} K_{\mathrm{N}} f_{\mathrm{N}} (K_{\mathrm{H}_2,\bullet-\mathrm{S}^{2-}} f_{\mathrm{H}_2})^{3/2} \left(1 - \frac{f_{\mathrm{T}}}{K_{\mathrm{eq}} f_{\mathrm{N}} f_{\mathrm{H}_2}^2}\right) C_* C_{\bullet-\mathrm{S}^{2-}}$	3-H-SA
$* \text{-} NH_3 + \bullet\text{-} S^{2-} H \rightleftharpoons * \text{-} T + \bullet\text{-} S^{2-}$	$R_{\mathrm{T},\bullet-\mathrm{S}^{2-}\mathrm{H}} = k_4 K_{\mathrm{N}\rightarrow\mathrm{NH}_3,\bullet-\mathrm{S}^{2-}} K_{\mathrm{N}} f_{\mathrm{N}} (K_{\mathrm{H}_2,\bullet-\mathrm{S}^{2-}} f_{\mathrm{H}_2})^2 \left(1 - \frac{f_{\mathrm{T}}}{K_{\mathrm{eq}} f_{\mathrm{N}} f_{\mathrm{H}_2}^2}\right) C_* C_{\bullet-\mathrm{S}^{2-}}$	4-H-SA

Where $C_{\mathrm{t},*} = C_* \left[1 + K_{\mathrm{N}} f_{\mathrm{N}} + \sqrt{K_{\mathrm{H}_2,*}} + \frac{K_{\mathrm{H}_2\mathrm{S}} f_{\mathrm{H}_2\mathrm{S}}}{\sqrt{K_{\mathrm{H}_2,\bullet-\mathrm{S}^{2-}} f_{\mathrm{H}_2}}} + K_{\mathrm{T}} f_{\mathrm{T}}\right], C_{\mathrm{t},\bullet-\mathrm{S}^{2-}} = C_{\bullet-\mathrm{S}^{2-}} (1 + \sqrt{K_{\mathrm{H}_2,\bullet-\mathrm{S}^{2-}} f_{\mathrm{H}_2}})$.

The surface concentrations of species in Eq. (23) are written as a function of known fugacities as follows:

$$C_{*-\mathrm{NH}_2} = K_{\mathrm{N}\rightarrow\mathrm{NH}_2} K_{\mathrm{N}} f_{\mathrm{N}} K_{\mathrm{H}_2} f_{\mathrm{H}_2} C_* \tag{24}$$

$$C_{*-\mathrm{NH}_3{}^-} = \frac{K_{\mathrm{T}} f_{\mathrm{T}} C_{*-\mathrm{H}^-}}{K_{\mathrm{NH}_3{}^-\rightarrow\mathrm{T}}} \tag{25}$$

$$C_{*-\mathrm{H}^-} = \frac{K_{\mathrm{H}_2} f_{\mathrm{H}_2} C_{\bullet-\mathrm{S}^{2-}} C_*}{C_{\bullet-\mathrm{S}^{2-}\mathrm{H}^+}} \tag{26}$$

This, together with the overall equilibrium coefficient, K_{eq}, leads to the actual rate equation for the third hydrogen species addition (hydride) as being rate determining:

$$R_{\mathrm{T}} = k_3 K_{\mathrm{N}\rightarrow\mathrm{NH}_2} K_{\mathrm{N}} K_{\mathrm{H}_2}^2 f_{\mathrm{N}} f_{\mathrm{H}_2}^2 \left(1 - \frac{f_{\mathrm{T}}}{K_{\mathrm{eq}} f_{\mathrm{N}} f_{\mathrm{H}_2}^2}\right) \times \frac{C_{\mathrm{t},*}^2}{\sqrt{\delta\mu}(\sqrt{\delta} + \sqrt{\mu})^2} \tag{27}$$

The entire set of rate equations derived assuming each hydrogen species addition as possible rate-determining step is shown in Tables 3 and 4.

5. Model regression and discussion

The qualitative behaviour of the various models is rather similar. Within the same type of reaction mechanism, the H_2 partial reaction order is the only distinctive feature and makes qualitative model discrimination difficult. As a result, model regression is required to discriminate among the various models.

5.1. Isothermal regression

In the first instance, model discrimination was carried out by performing isothermal parameter estimation using the 16 rate equations and the experimental data obtained at 553 K. The number of experiments at this temperature amounted to 80.

It can be observed from Tables 3 and 4 that models based on the homolytic mechanism contain six coefficients, i.e., one rate coefficient and five chemisorption coefficients, whereas models based on the heterolytic mechanism only 5. For simplicity, a composite rate coefficient is defined as the product of the real rate coefficient and the equilibrium and chemisorption coefficients of the elementary steps involved in the formation of the species consumed in the rate-determining step.

After regression using the experimental data obtained at the reference temperature, some models could be discarded, vide Table 5. The rate equations corresponding to a hydrogenation mechanism in which the rate-determining step was a hydrogen addition from a sulphur anion, i.e., from $^{\bullet}$–S^{2-}, either as atomic hydrogen or as a proton, were discarded because of the low F-value related to the global significance of the regression or because fewer parameters could be estimated significantly. In addition, the models derived assuming the first and the second hydrogen additions as RDS can be discarded also based on the low F-value and the low number of parameters significantly estimated. Within the remaining models, the best results were obtained with models 3-H-CUS and 3-Hydride. These two models have in common that the third hydrogen addition is considered as rate determining.

The isothermal regression and model discrimination allows to draw two major conclusions. First, hydrogen chemisorbed on sulphur anions appear not to be involved in the rate-determining step in aromatic hydrogenation on a NiMo sulphide catalyst. It may, however, well be that hydrogen addition from sulphur

Table 4
Rate equations derived from heterolytic mechanism assuming each hydrogen addition as possible rate-determining step

Hydrogenation network assuming a hydride addition first (*–H$^-$)		
$*\text{-}N + *\text{-}H \rightleftharpoons * \text{-}NH + *$	$R_{NH^-,*-H^-} = \frac{k_1 K_N f_N K_{H_2} f_{H_2} (1-(f_T/K_{eq} f_N f_{H_2}^2)) C_{t,*}^2}{\sqrt{\mu\delta}(\sqrt{\mu}+\sqrt{\delta})^2}$	1-Hydride
$*\text{-}NH + *\text{-}H \rightleftharpoons *\text{-}NH_2 + *$	$R_{NH_2,\bullet-S^{2-}H^+} = \frac{k_2 K_{N\to NH^-} K_N f_N K_{H_2} f_{H_2} (1-(f_T/K_{eq} f_N f_{H_2}^2)) C_{t,*}^2}{(\sqrt{\mu}+\sqrt{\delta})^2}$	2-Proton
$*\text{-}NH_2 + *\text{-}H \rightleftharpoons *\text{-}NH_3 + *$	$R_{NH_3^-,*-H^-} = \frac{k_3 K_{N\to NH_2} K_N f_N (K_{H_2} f_{H_2})^2 (1-(f_T/K_{eq} f_N f_{H_2}^2)) C_{t,*}^2}{\sqrt{\mu\delta}(\sqrt{\mu}+\sqrt{\delta})^2}$	3-Hydride
$*\text{-}NH_3 + *\text{-}H \rightleftharpoons *\text{-}T + *$	$R_{T,\bullet-S^{2-}H^+} = \frac{k_4 K_{N\to NH_3^-} K_N f_N (K_{H_2} f_{H_2})^2 (1-(f_T/K_{eq} f_N f_{H_2}^2)) C_{t,*}^2}{(\sqrt{\mu}+\sqrt{\delta})^2}$	4-Proton
Hydrogenation network assuming a proton addition first ($^\bullet$–S^{2-}H$^+$)		
$*\text{-}N + \bullet\text{-}S^{2-}H \rightleftharpoons *\text{-}NH + \bullet\text{-}S^{2-}$	$R_{NH^+,\bullet-S^{2-}H^+} = k_1 K_N f_N \left(1 - \frac{f_T}{K_{eq} f_N f_{H_2}^2}\right) C_{t,*}^2 \frac{\sqrt{\mu\delta}}{\delta(\sqrt{\delta}+\sqrt{\mu})^2}$	1-Proton
$*\text{-}NH + \bullet\text{-}S^{2-}H \rightleftharpoons *\text{-}NH_2 + \bullet\text{-}S^{2-}$	$R_{NH_2,*-H^-} = k_2 K_{N\to NH^+} K_N f_N K_{H_2} f_{H_2} \left(1 - \frac{f_T}{K_{eq} f_N f_{H_2}^2}\right) C_{t,*}^2 \frac{1}{\delta(\sqrt{\delta}+\sqrt{\mu})^2}$	2-Hydride
$*\text{-}NH_2 + \bullet\text{-}S^{2-}H \rightleftharpoons *\text{-}NH_3 + \bullet\text{-}S^{2-}$	$R_{NH_3^+,\bullet-S^{2-}H^+} = k_3 K_{N\to NH_2} K_N f_N K_{H_2} f_{H_2} \left(1 - \frac{f_T}{K_{eq} f_N f_{H_2}^2}\right) C_{t,*}^2 \frac{\sqrt{\mu\delta}}{\delta(\sqrt{\delta}+\sqrt{\mu})^2}$	3-Proton
$*\text{-}NH_3 + \bullet\text{-}S^{2-}H \rightleftharpoons *\text{-}T + \bullet\text{-}S^{2-}$	$R_{T,*-H^-} = k_4 K_{N\to NH_3^+} K_N f_N K_{H_2}^2 f_{H_2}^2 \left(1 - \frac{f_T}{K_{eq} f_N f_{H_2}^2}\right) C_{t,*}^2 \frac{1}{\delta(\sqrt{\delta}+\sqrt{\mu})^2}$	4-Hydride

Where $\delta = 1 + K_N f_N + K_T f_T$ and $\mu = K_{H_2} f_{H_2} + K_{H_2S} f_{H_2S}$.

anions occurs in the potentially very fast elementary steps. Second, the rate-determining step appears to occur in the second half of the hydrogenation pathway, i.e., the third hydrogen addition, rather than the first or the second. This is in line with previous modelling efforts on toluene hydrogenation on Pt [42] and can be interpreted in terms of breaking the aromatic character of the reactant upon chemisorption on the catalyst surface. A rate-determining step further in the hydrogenation pathway was also found by, among others, Nakano and Kusunoki [43], Nakano et al. [44] and Yoon and Vannice [45].

5.2. Non-isothermal regression

The further model discrimination between the two remaining models, denoted as 3-H-CUS and 3-Hydride, was performed by reparameterized non-isothermal regression using the entire set of experimental data. The temperature dependence of the coefficients doubles the number of parameters to be determined as compared to isothermal regression. To keep the number of parameters to be estimated reasonable, the pre-exponential factors of the rate and chemisorption coefficients were calculated using statistical thermodynamics and transition state theory [46]. Based on the assumed mobility for the species involved as reactant and activated complex, the pre-exponential factors can be obtained from the corresponding partition functions. Performing these calculations for different possible mobilities of the species involved leads to the ranges mentioned in Table 6. Chemisorption entropies are expected to be negative due to the loss in translational and rotational degrees of freedom of the fluid

Table 5
Summary of results of isothermal model regression for naphthalene hydrogenation over sulphided NiMo using data obtained at 553 K

Mechanism	Model	F-value	Number of parameters significantly estimated
Homolytic: *–H addition	1-H-CUS	1178	5/9
	2-H-CUS	842	6/9
	3-H-CUS	1738	6/9
	4-H-CUS	1613	5/9
Homolytic: $^\bullet$–S^{2-}H addition	1-H-SA	499	6/9
	2-H-SA	1269	4/9
	3-H-SA	1334	6/9
	4-H-SA	1169	6/9
Heterolytic: hydride (*–H–) addition first	1-Hydride	611	5/8
	2-Proton	1119	5/8
	3-Hydride	2018	5/8
	4-Proton	1027	5/8
Heterolytic: proton ($^\bullet$–S^{2-}H$^+$) addition first	1-Proton	287	4/8
	2-Hydride	1968	3/8
	3-Proton	890	4/8
	4-Hydride	1382	5/8

Data amounted to 80 experiments.

Table 6
Range of pre-exponential factors and the corresponding entropy range of the chemisorption coefficients estimated based on statistical thermodynamics [46]

Coefficient	Range of pre-exponential factors (bar^{-1})	Range of ΔS_{ads} ($J\ mol^{-1}\ K^{-1}$)
K_A	$10^{-10}/10^{-5}$	−191/−95.7
K_B	$10^{-10}/1$	−191/0.0

A: naphthalene and tetralin (molecular adsorption); B: hydrogen and hydrogen sulphide (dissociative chemisorption).

phase molecules upon chemisorption onto the catalytic surface. In the case of dissociative chemisorption, i.e., for hydrogen and hydrogen sulphide, the dissociative character has a positive contribution to the total chemisorption entropy. As a result, no change in entropy for the overall process is set as the upper limit in hydrogen and hydrogen sulphide chemisorption. Several consistent set of values for the pre-exponential factors were tested in regressions.

The highest F-value for the global significance of the regression was obtained for the model considering heterolytic dissociation, 3263, compared to 2610 for the model considering homolytic dissociation. With both models three parameters could be significantly estimated, i.e., the composite activation energy and the chemisorption enthalpies for H_2S and H_2 on CUS. The corresponding parity diagrams between the calculated and experimental tetralin molar outlet flow rates obtained for both models are shown in Figs. 6 and 7. A good qualitative description of the experimental data is obtained with both models making difficult the model discrimination based on these diagrams.

The pre-exponential factor and chemisorption entropies used in the best regression are listed in Table 7. The estimated parameter values are reported in Table 8. The 95% confidence intervals of the parameter estimates for both models strongly overlap and do not allow a discrimination between the two models. The naphthalene and tetralin chemisorption enthalpies and that for H_2 chemisorption on sulphur anions could not be estimated significantly. Although not statistically significant, the removal of these parameters from the model visually affected the parity diagram and, hence, in the final regression these parameters were fixed at average values obtained during the regression procedure using various initial parameter guesses. The trend among the hydrocarbon chemisorption enthalpies indicates that naphthalene is more strongly bound to the surface than tetralin which is line with other hydrogenation studies of these molecules [47,48].

Table 7
Pre-exponential factor of the composite rate coefficient and chemisorption entropies fixed and used in the best non-isothermal regression for the remaining models

Parameter	3-H-CUS	3-Hydride
A^{comp} ($kmol\ s^{-1}\ kg^{-1}\ bar^{-2.5}$)	38.0E−06	7.0E−06
ΔS°_{N} ($J\ mol^{-1}\ K^{-1}$)	−129	−129
$\Delta S^{\circ}_{H_2,*}$ ($J\ mol^{-1}\ K^{-1}$)	−156	−161
$\Delta S^{\circ}_{H_2,\bullet-S^{2-}}$ ($J\ mol^{-1}\ K^{-1}$)	−106	
$\Delta S^{\circ}_{H_2S}$ ($J\ mol^{-1}\ K^{-1}$)	−231	−189
ΔS°_{T} ($J\ mol^{-1}\ K^{-1}$)	−97.1	−97.1

A^{comp} is the composite pre-exponential factor of $k^{comp} = k_{NH_2\rightarrow NH_3} K_N K^{3/2}_{H_2,*}$ in model 3-H-CUS, or $k^{comp} = k_{NH_2\rightarrow NH_3} \cdot K_{N\rightarrow NH_2} K_N K^2_{H_2}$ in model 3-Hydride.

Table 8
Estimated composite activation energy and chemisorption enthalpy values with their corresponding 95% confidence interval obtained in non-isothermal regression with remaining models

Parameter	3-H-CUS	3-Hydride
E^{comp}_a ($kJ\ mol^{-1}$)	−41.5 ± 17.5	−37.9 ± 13.2
ΔH°_{N} ($kJ\ mol^{-1}$)	−48.0	−48.0
$\Delta H^{\circ}_{H_2,*}$ ($kJ\ mol^{-1}$)	−80.0 ± 32.1	−82.5 ± 27.7
$\Delta H^{\circ}_{H_2,\bullet-S^{2-}}$ ($kJ\ mol^{-1}$)	−47.0	
$\Delta H^{\circ}_{H_2S}$ ($kJ\ mol^{-1}$)	−128 ± 20.8	−109 ± 19.7
ΔH°_{T} ($kJ\ mol^{-1}$)	−40.0	−40.0

E^{comp}_a is the composite activation energy of $k^{comp} = k_{NH_2\rightarrow NH_3} K_{N\rightarrow NH_2} K_N K^{3/2}_{H_2,*}$ in model 3-H-CUS, or $k^{comp} = k_{NH_2\rightarrow NH_3} \cdot K_{N\rightarrow NH_2} K_N K^2_{H_2}$ in model 3-Hydride.

The chemisorption enthalpies for naphthalene and tetralin could not be estimated significantly with either of the two

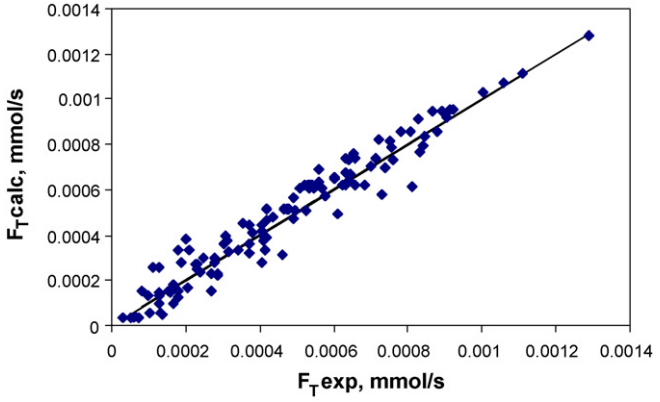

Fig. 6. Parity diagram of experimental vs. calculated outlet tetralin molar flow rate obtained from model regression at non-isothermal conditions. Calculated responses using the set of parameters in Tables 7 and 8 and the net rate of hydrogenation denoted as model 3-H-CUS in Table 4.

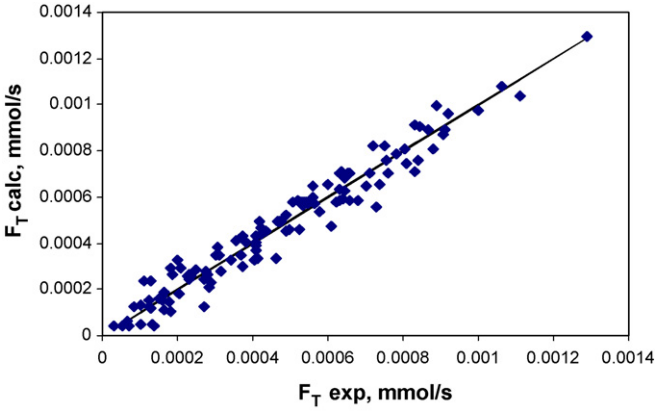

Fig. 7. Parity diagram of experimental vs. calculated outlet tetralin molar flow rate obtained from model regression at non-isothermal conditions. Calculated responses using the set of parameters in Tables 7 and 8 and the net rate of hydrogenation denoted as model 3-Hydride in Table 4.

Table 9
Comparison of fractional surface coverage calculated by regression using models 3 and 11

Variable	3-H-CUS			3-Hydride		
	Θ_{free}	Θ_{H}	Θ_{H_2S}	Θ_{free}	Θ_{H}	Θ_{H_2S}
Reference conditions	0.42	0.46	0.12	0.50	0.12	0.38
Temperature (K)						
523	0.19	0.55	0.26	0.22	0.16	0.62
583	0.65	0.31	0.04	0.78	0.06	0.16
H_2/H_2S (mol mol^{-1})						
20	0.38	0.42	0.20	0.38	0.09	0.54
10	0.33	0.35	0.32	0.26	0.05	0.69
5	0.27	0.26	0.47	0.17	0.03	0.80

Table 10
Hydrogen and hydrogen sulphide chemisorption coefficients calculated at 573 K with the set of parameters of Tables 6 and 7 and literature reported

Parameter	3-H-CUS (NiMo, bar^{-1})	3-Hydride (NiMo, bar^{-1})	HDS/DBT [21] (CoMo, bar^{-1})	HDN/PYR [49] (NiMo, bar^{-1})	K_{H_2S} [50] (CoMo, bar^{-1})
$K_{H_2,*}$	0.13	0.01	0.0056	n.s.	
$K_{H_2,\bullet-S^{2-}}$	0.05	–	0.028	0.09	
K_{H_2S}	0.43	1.18	2.52	0.19	735

models, vide Table 8. This indicates that the surface concentration of these species is considerably lower than that of the H_2 and H_2S dissociated species. The H_2 chemisorption enthalpy on sulphur anions not being significantly estimated is in agreement with the intermediate conclusion after the isothermal regression that these species are not involved a rate-determining step.

The calculated surface distribution of species for some experiments obtained from the optimal model regression is given in Table 9. An opposite result of surface concentration between hydrogen and hydrogen sulphide is obtained from the calculated surface coverage with both models and can be related to the different shape of the denominator. The values obtained with model 3-Hydride intuitively fit best into the interpretation of the experimentally observed trends, i.e., the inhibitory effect of H_2S, because the sulphydril is calculated to be the most abundant surface intermediate (MASI). However, the parameter combination obtained with model 3-H-CUS shows that the rationalization of the experimental data does not necessarily require the sulphydril species as the most abundant surface intermediates on the CUS, but that also hydrogen atoms might be the most abundant surface intermediates. Further discrimination between the two kinetic models will require additional experimental data in an even wider range of operating conditions than already examined now.

The current results are in good agreement with those reported in literature. The chemisorption coefficients for H_2 and H_2S were calculated at 573 K and confronted with reported values for hydrodesulphurization of benzothiophene (HDS) on $CoMo/Al_2O_3$ [21], for hydrodenitrogenation of pyridine (HDN) on $NiMo/Al_2O_3$ [49] and from a thermodynamic modelling study of H_2S chemisorption on $CoMo/Al_2O_3$ [50], vide Table 10. Those studies of HDS and HDN constructed models based on a homolytic dissociation of H_2 and H_2S similar to the current model 3-H-CUS. The values obtained on the NiMo catalyst are in line with the values obtained in this work using model 3-H-CUS. Co as promoter metal leads to a H_2S chemisorption coefficient which is an order of magnitude higher than that with Ni as promoter, whereas the hydrogen chemisorption coefficient with Co as promoter is much lower than with Ni as promoter. The thermodynamic study of H_2S sorption confirms the higher chemisorption coefficient for H_2S with Co as promoter metal. The differences between the values reported by Vanrysselberghe and Froment [21] and Echard and Leglise [50] originate from different assumptions with respect to the mobility of the surface intermediated.

The chemisorption enthalpy for H_2S obtained in the current study, i.e., -128 and -109 kJ mol^{-1} for the homolytic and heterolytic models, respectively, is in agreement with that reported by Borgna et al. [51], which is -117 kJ mol^{-1} over planar sulphided $NiMo/SiO_2$ during HDS of thiophene at 573–673 K and atmospheric pressure. The difference in catalyst support used by Borgna et al. [51] and in this work may explain the intermediate value reported by Borgna et al. compared to the values obtained in this work.

6. Conclusions

Naphthalene hydrogenation is highly selective to tetralin on the investigated commercial $NiMo/\gamma Al_2O_3$ catalyst. Intrinsic kinetics can be measured in a wide range of operating conditions. The naphthalene hydrogenation rate over a sulphided NiMo was found to be limited by the addition of a hydrogen species chemisorbed on coordinatively unsaturated metal ion sites. The third hydrogen addition has been identified as the rate-determining step.

The current kinetic data set did not allow to significantly discriminate between a homolytic or heterolytic reaction

mechanism. The strength of the hydrogen and hydrogen sulphide chemisorption is slightly different depending on the type of dissociation. As a result, whereas in the heterolytic mechanism the sulphydril species was found to be the most abundant surface intermediate, the homolytic mechanism puts the hydrogen atoms forward as the most abundant surface species. Both models agree, however, that hydrocarbon species concentrations on the catalyst surface are negligible and that hydrogen chemisorbed on sulphur anions is not involved in the rate-determining step.

References

[1] Refining Processes 2000 (entire issue), Hydrocarbon Processing 79 (2000).
[2] H. Topsoe, J. Catal. 216 (1–2) (2003) 155–164.
[3] A.N. Startsev, I.I. Zakharov, V.N. Parmon, J. Mol. Catal. A: Chem. 192 (1–2) (2003) 113–127.
[4] C. Thomas, L. Vivier, J.L. Lemberton, S. Kasztelan, G. Perot, J. Catal. 167 (1) (1997) 1–11.
[5] L.S. Byskov, J.K. Norskov, B.S. Clausen, H. Topsoe, J. Catal. 187 (1999) 109–122.
[6] P. Raybaud, J. Hafner, G. Kresse, S. Kasztelan, H. Toulhoat, J. Catal. 189 (2000) 129–146.
[7] A. Travert, H. Nakamura, R.A. van Santen, S. Cristol, J.F.E. Payen, J. Am. Chem. Soc. 124 (2002) 7084.
[8] M. Sun, A.E. Nelson, J. Adjaye, Catal. Today 105 (2005) 36–43.
[9] M. Sun, J. Adjaye, A.E. Nelson, Appl. Catal. A: Gen. 263 (2004) 131–143.
[10] R. Prins, V.H.J. de Beer, G.A. Somorjai, Catal. Rev.-Sci. Eng. 31 (1989) 1.
[11] H. Topsoe, B.S. Clausen, F.E. Massoth, Hydrotreating Catalysis, Springer-Verlag, Berlin, 1996.
[12] J.F. Paul, E. Payen, J. Phys. Chem. B 107 (2003) 4057–4064.
[13] M. Breysse, E. Furimsky, S. Kasztelan, M. Lacroix, G. Perot, Catal. Rev. 44 (4) (2002) 651–735.
[14] J. Polz, H. Zeilinger, B. Muller, H. Knozinger, J. Catal. 120 (1) (1989) 22–28.
[15] A. Sierraalta, F. Ruette, J. Mol. Catal. A: Chem. 109 (3) (1996) 227–238.
[16] E.J.M. Hensen, G.M.H. Lardinois, V.H.J. de Beer, J.A.R. van Veen, R.A. van Santen, J. Catal. 187 (1) (1999) 95–108.
[17] S. Cristol, J.F. Paul, E. Payen, D. Bougeard, S. Clemendot, F. Hutschka, J. Phys. Chem. B 104 (2000) 11220–11229.
[18] S. Kasztelan, D. Guillaume, Ind. Eng. Chem. Res. 33 (1994) 203–210.
[19] S. Blanchin, P. Galtier, S. Kasztelan, S. Kressman, H. Penet, G. Perot, J. Phys. Chem. A (2001) 10860–10866.
[20] A. Guevara, R. Bacaud, M. Vrinat, Appl. Catal. A: Gen. 253 (2003) 515–526.
[21] V. Vanrysselberghe, G.F. Froment, Ind. Eng. Chem. Res. 35 (1996) 3311–3318.
[22] V. Vanrysselberghe, R. Le Gall, G.F. Froment, Ind. Eng. Chem. Res. 37 (1998) 1235–1242.
[23] V. Vanrysselberghe, G.F. Froment, Ind. Eng. Chem. Res. 37 (1998) 4231–4240.
[24] A. Stanislaus, B.H. Cooper, Catal. Rev. Sci. Eng. 36 (1) (1994) 75–123.
[25] Health Assessment Document for Diesel Engine Exhaust, EPA, US, 2002.
[26] J.A. Muñoz Arroyo, G.G. Martens, G.F. Froment, G.B. Marin, P.A. Jacobs, J.A. Martens, Appl. Catal. A: Gen. 192 (1) (2000) 9–22.
[27] J.L. Dierickx, P.M. Plehiers, G.F. Froment, J. Chromatogr. 362 (1986) 155–174.
[28] B.M. Vogelaar, P. Steiner, A.D. van Langeveld, S. Eijbouts, J.A. Moulijn, Appl. Catal. A: Gen. 251 (2000) 85–92.
[29] B.E. Poling, J.M. Prausnitz, J.P. O'Connell, The Properties of Gases and Liquids, fifth ed., McGraw-Hill, New York, 2000.
[30] F. Kapteijn, G.B. Marin, J.A. Moulijn, Catalysis: An Integrated Approach to Homogeneous, Heterogeneous and Industrial Catalysis, Elsevier, Amsterdam, 1993.
[31] J.J. Carberry, Chemical and Catalytic Reaction Engineering, McGraw-Hill, New York, 1976.
[32] D.E. Mears, J. Catal. 20 (1971) 127.
[33] P.B. Weisz, C.D. Prater, Advances in Catalysis, Academic Press, New York, 1954, p. 143.
[34] B.W. Hoffer, P.H.J. Schoenmakers, P.R.M. Mooijman, G.M. Hamminga, R.J. Berger, A.D. van Langeveld, J.A. Moulijn, Chem. Eng. Sci. 59 (2004) 259–269.
[35] G.F. Froment, L.H. Hosten, in: J. Anderson, M. Boudart (Eds.), Catalysis-Science and Technology, vol. 2, Springer Verlag, Berlin, 1981 , pp. 97–170 (Chapter 3).
[36] J.W. Thybaut, C.S. Laxmi Narasimhan, G.B. Marin, Catal. Today 111 (2006) 94–102.
[37] Netlib, http://www.netlib.org.
[38] K. Hou, R. Hughes, Chem. Eng. J. 82 (2001) 311–328.
[39] J. Xu, G.F. Froment, AIChE J. 35 (1989) 88–96.
[40] G.F. Froment, K. Bishop (Eds.), Chemical Reactor Analysis and Design, John Wiley & Sons, 1990.
[41] J. Ancheyta, G. Marroquín, M.J. Angeles, M.J. Macías, I. Pitault, M. Forissier, D. Morales, Energy Fuels 16 (2002) 1059–1067.
[42] J.W. Thybaut, M. Saeys, G.B. Marin, Chem. Eng. J. 90 (2002) 117–129.
[43] K. Nakano, K. Kusunoki, Chem. Eng. Commun. 34 (1985) 99–109.
[44] K. Nakano, Y. Fueda, T. Uchino, K. Kusunoki, Chem. Eng. Jpn. 15 (1982) 397–399.
[45] K.J. Yoon, M.A. Vannice, J. Catal. 82 (1983) 457–468.
[46] D.A. Dumesic, D.F. Rudd, L.M. Aparicio, J.E. Kekoske, A.A. Treviño, The Microkinetics of Heterogeneous Catalysis, American Chemical Society, Washington, DC, 1993.
[47] P.A. Rautanen, M.S. Lylykangas, J.R. Aittamaa, A.O.I. Krause, Stud. Surf. Sci. Catal. 133 (2001) 309–316.
[48] P.A. Rautanen, J.R. Aittamaa, A.O.I. Krause, Chem. Eng. Sci. 56 (2001) 1247–1254.
[49] R. Pille, G. Froment, Stud. Surf. Sci. Catal. 106 (1997) 403–413.
[50] M. Echard, J. Leglise, Thermochim. Acta 379 (1–2) (2001) 241–254.
[51] A. Borgna, E.J.M. Hensen, J.A.R. van Veen, J.W. Niemantsverdriet, J. Catal. 221 (2004) 541–548.